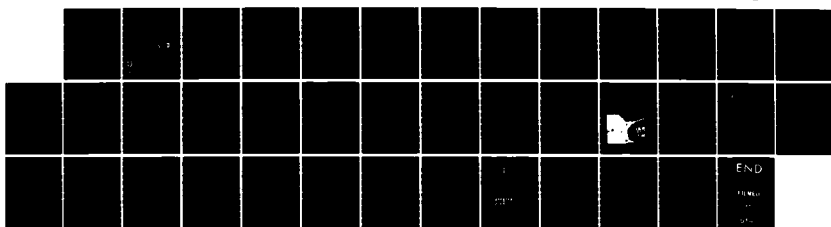


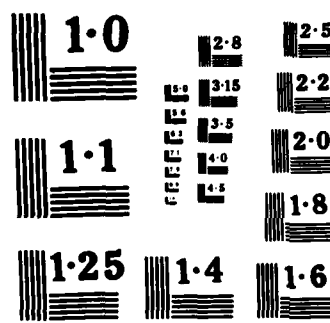
AD-A163 240 PERFORMANCE TEST OF LASER VELOCIMETER SYSTEM FOR THE 1/1
LANGLEY 16-FOOT TUNNEL (U) NATIONAL AERONAUTICS AND
SPACE ADMINISTRATION HAMPTON VA LANG.
UNCLASSIFIED J F MEYERS ET AL. DEC 85 NASA-L-15948

F/G 14/2

NL



END
DRAFT
01/01



NATIONAL BUREAU OF STANDARDS
MICROCOPY RESOLUTION TEST CHART

NASA
Technical
Paper
2502

2

AVSCOM
Technical
Report
85-B-4

December 1985

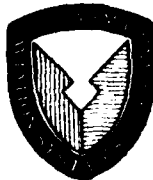
AD-A163 240

Performance Test of
Laser Velocimeter System
for the Langley 16-Foot
Transonic Tunnel

James F. Meyers,
William W. Hunter, Jr.,
David E. Reubush,
Cecil E. Nichols, Jr.,
Timothy E. Hepner,
and Joseph W. Lee

DTIC
ELECTED
JAN 22 1986

DTIC FILE COPY



NASA

86 1 22 076

**NASA
Technical
Paper
2502**

**AVSCOM
Technical
Report
85-B-4**

1985

Performance Test of Laser Velocimeter System for the Langley 16-Foot Transonic Tunnel

James F. Meyers,
William W. Hunter, Jr.,
David E. Reubush,
and Cecil E. Nichols, Jr.
*Langley Research Center
Hampton, Virginia*

Timothy E. Hepner
*Aerostructures Directorate
USAARIA-AVSCOM
Langley Research Center
Hampton, Virginia*

Joseph W. Lee
*Langley Research Center
Hampton, Virginia*

Accession For	
NTIS	CRA&I
DTIC	TAB
Unannounced	
Justification	
By _____	
Distribution / _____	
Availability Codes	
Dist	Avail and/or Special
A-1	



NASA

National Aeronautics
and Space Administration

Scientific and Technical
Information Branch

ABSTRACT

An investigation in the Langley 16-Foot Transonic Tunnel has been conducted in which a laser velocimeter was used to measure free-stream velocities from Mach 0.1 to 1.0 and the flow velocities along the stagnating streamline of a hemisphere-cylinder model at Mach 0.8 and 1.0. The flow velocity was also measured at Mach 1.0 along the line 0.533 model diameters below the model. These tests determined the performance characteristics of the dedicated two-component laser velocimeter at flow velocities up to Mach 1.0 and the effects of the wind tunnel environment on the particle-generating system and on the resulting size of the generated particles. To determine these characteristics, the measured particle velocities along the stagnating streamline at the two Mach numbers were compared with the theoretically predicted gas and particle velocities calculated using a transonic potential flow method. Through this comparison the mean detectable particle size ($2.1 \mu\text{m}$) along with the standard deviation of the detectable particles ($0.76 \mu\text{m}$) was determined; thus the performance characteristics of the laser velocimeter were established.

INTRODUCTION

The need to make nonintrusive velocity measurements of transonic flows has prompted the construction of a dedicated two-component laser velocimeter for the Langley 16-Foot Transonic Tunnel. The purpose of this paper is to describe the design requirements, the resulting system, and its performance characteristics. The results of the system performance tests include the effects of the wind tunnel environment on the particle-generating system, the resulting particle size distribution, and the effects of this distribution on the accuracy of the velocity measurements.

The laser velocimeter is a two-component optical system using color separation and operated in the coaxial backscatter configuration. Bragg cells were included in both components of the system to yield full measurement directionality in the plane orthogonal to the optical axis. (The Bragg cell in the component measuring streamwise velocity, the U-component, was removed in the present study, since reversed flows would not be present.) The optical system is mounted on a bi-directional mechanical traversing mechanism to move the sample volume along the vertical Y-axis and the horizontal tunnel X-axis, and a zoom lens is used to move the sample volume along the horizontal optical Z-axis. The entire system was located within the plenum chamber surrounding the test section. The particle-generating system is an atomizer that used micrometer-sized hydrous aluminum silicate (kaolin) particles suspended in ethanol. The particle-generating system was mounted on the final set of turning vanes upstream of the test section.

The performance tests of the laser velocimeter consisted of measuring the velocity of the kaolin particles along the stagnating streamline of a hemisphere-cylinder model at Mach 0.8 and 1.0 and comparing these results with gas velocities theoretically predicted with a potential flow method. Then the theoretical particle velocity profiles, based on these gas velocity profiles were calculated as a function of particle size, and the results compared with the measured velocities in

a least squares fashion to determine the average size of the particles present in the flow that are detected by the laser velocimeter. The results of this analysis provided an indication of the performance characteristics of the laser velocimeter and the capabilities of the particle-generating system using kaolin particles within the wind tunnel environment.

SYMBOLS

D	model diameter, cm
g	acceleration due to gravity, m/sec^2
LV	laser velocimeter
M	Mach number
U	velocity component in streamwise direction, m/sec
\bar{U}	mean value of U , m/sec
V	velocity component in vertical direction, m/sec
\bar{V}	mean value of V , m/sec
x,y	streamwise and vertical coordinates with origin at nose of model, cm
$\bar{\alpha}$	mean flow angle in UV-plane, deg
σ_α	standard deviation of α , deg
σ_U	standard deviation of U , m/sec
σ_V	standard deviation of V , m/sec
σ_U/\bar{U}	local turbulence intensity in U -component, percent
σ_V/\bar{U}	local turbulence intensity in V -component, percent

Subscripts:

corr	corrected
gas	theoretical gas velocity
meas	measured with laser velocimeter
part	theoretical particle velocity

APPARATUS

Wind Tunnel

The Langley 16-Foot Transonic Tunnel is a closed-circuit, continuous-flow, fan-driven, atmospheric wind tunnel, described in reference 1 and shown schematically in figure 1. The test medium is air and the tunnel is equipped with an air exchange for cooling. The wind tunnel has a Mach number range up to 1.3 and an average Reynolds number of 13×10^6 per meter at Mach numbers above 0.6. The octagonal test section has movable walls to minimize the axial Mach number gradient and is slotted for removal of the boundary layer by evacuation of the surrounding 9.75-m-diameter plenum at Mach numbers above 1.03. The approximate ambient conditions within the plenum chamber at Mach 1.0 are a pressure of 0.5 atm, a temperature of 50°C, and acoustic noise of 150 dBm. The structural members within the plenum chamber are subjected to vibration levels of up to 5g. An optical quality window installed in the test section wall provides optical access to the test section from the plenum. This window is made of BK-7 glass and has a clear viewing area of 1.27 m by 0.91 m and a thickness of 6.35 cm. The optical quality of the window surface is maintained by installing it only for laser velocimeter measurements.

Test Model

The purpose of the performance test program was to demonstrate that the laser velocimeter will accurately measure velocity in flow fields up to Mach 1.0. The accuracy of these measurements depends on the size of the particles used to generate them. The most straightforward method to determine the size of these particles is to probe a known strongly decelerating (or accelerating) flow field where the particle size may be inferred by comparing the velocity measurements with theoretically predicted velocities for various particle sizes. One such flow field is found along the stagnating streamline of a hemisphere. Therefore a hemisphere 19.05 cm in diameter followed by a 10.16-cm-long cylinder was chosen as the test model. The model was sting mounted on the tunnel centerline at an angle of attack of 0°. The model installed within the test section is shown in figure 2.

Laser Velocimeter System

The performance requirements of the dedicated laser velocimeter system for the Langley 16-Foot Transonic Tunnel are as follows:

1. Capability to measure free-stream velocities from 70 m/sec to 420 m/sec with an accuracy of 1 percent in the mean velocity.
2. Bidirectional velocity measurement capability along the tunnel axis (U-component) and in the vertical direction (V-component).
3. Maximum size of ellipsoidal sample volume of 1 mm in diameter and 1 cm in length.
4. Movement of the sample volume within a cube 1.0 m by 0.6 m by 2.0 m (axial, vertical, and cross tunnel directions, respectively) centered on the tunnel centerline.

The laser velocimeter system designed to meet these performance requirements, and the subject of the present study, is a two-component optical system using color separation of the components and configured in the coaxial backscatter mode. The specific system characteristics are given in table I and the optical system is shown schematically in figure 3. Each component contains a Bragg cell to obtain velocity directionality, with the Bragg cell in the U-component removable to extend the range of maximum velocity (removed for the present study). The system uses high-speed burst counter signal processing, and a data acquisition buffer system (ref. 2) serves as the interface between the counters and the host minicomputer system. This system is theoretically capable of measuring U-component velocities from nominally 0 m/sec to 933 m/sec, and with insertion of the Bragg cell, from -187 m/sec to 373 m/sec, and V-component velocities from -187 m/sec to 187 m/sec. The resulting ellipsoidal sample volume (measured to the $1/e^2$ power points) is 0.31 mm in diameter by 6.1 mm in length at the tunnel centerline. The focal length of the system is controlled by a zoom lens that moves the sample volume in the cross-tunnel direction ± 1.0 m about the tunnel centerline. At the near focal point the sample volume dimensions are 0.35 mm and 4.9 mm, and at the far focal point they are 0.97 mm and 11.6 mm. The sample volume is moved in the remaining two directions by a bidirectional mechanical traversing mechanism with a window-limited scan of 1.02 m horizontally along the tunnel centerline and 0.66 m vertically with a resolution of 0.5 mm. The laser velocimeter system was aligned with the vertical laser beams (V-component) lying along the axis of gravity determined by a plumb bob and the horizontal beams (U-component) orthogonal to the vertical axis determined by a large right triangle with an estimated precision of 0.1° . The traversing mechanism and zoom lens were adjusted to a reference point at the center surface pressure part on the nose of the model.

Theoretical Simulation of the Proposed Laser Velocimeter

This optical system was modeled with the computer simulation given in reference 3 to determine its sensitivity as a function of particle size at the tunnel centerline focal distance. The particle velocity was chosen to be 420 m/sec and the particle material chosen to be hydrous aluminum silicate (kaolin). The laser velocimeter sensitivity factor (probability of making a measurement) was formulated by first determining whether a particle of given size passing through the center of the sample volume would yield a velocity measurement. If so, then it was determined how far away from the center the particle could pass and still yield a measurement. This was done in the following manner.

The calculation of the measurement probability begins with determination of the electromagnetic field resulting from the scatter of light from a particle of a given size (described by Mie in ref. 4) as it passes through each of the pair of laser beams comprising the sample volume. The interaction between the two scattered fields is calculated over the collecting solid angle of the laser velocimeter using the method described in reference 5 to yield the optical transfer function, which is used along with the Gaussian intensity profile of the laser beams to obtain the theoretical signal burst. This burst is integrated and used to drive a Poisson random number generator to yield a Monte Carlo simulation of photon arrivals at the photocathode surface of the photomultiplier. The photons are convolved with the photomultiplier transfer function to obtain the electronic signal burst. The burst is then input to a model of a high-speed burst counter with double threshold detection circuits and 5:8 count comparison to determine whether the signal has sufficient

amplitude to yield a velocity measurement. If the signal, following band-pass filtering, does not have sufficient amplitude for 10 consecutive cycles to cross the thresholds with sufficient signal-to-noise ratio to satisfy the 5:8 comparison test, a measurement cannot be made and the sensitivity factor is zero for that particle size. If the signal is accepted by the counter, the amplitude of the signal is reduced exponentially until the signal fails to be accepted by the counter. The amount of reduction in amplitude corresponds to a distance from the center of the sample volume in accordance with the Gaussian intensity profile of the laser beams. A sensitivity factor of unity is arbitrarily assigned when the distance from the center of the sample volume corresponds to the sample volume radius, defined by the intensity being $1/e^2$ of the intensity at the center.

The choice of particle sizes to be used in the simulation is established by measuring the size distribution of the kaolin particles to be used in the wind tunnel. The particles were measured in the laboratory by suspending the kaolin in ethanol and spraying the mixture through a fluid atomizer (ref. 6), in order to evaporate the ethanol and leave the solid kaolin behind. These particles were then sampled by an aerodynamic particle size analyzer (ref. 7). The aerodynamic size however is not the physical size of the particle, but is larger by a factor equal to the square root of particle's specific gravity (ref. 8). Therefore with a specific gravity of 2.58, the kaolin particle size results presented in figure 4(a) have been reduced by 62.3 percent to obtain the particle sizes to be tested by the laser velocimeter simulation program. The resulting sensitivity factors corresponding to the appropriate particle sizes are presented in figure 4(b). Multiplying the particle size distribution (fig. 4(a)) by the corresponding sensitivity factor profile (fig. 4(b)) yields the detectable particle size distribution (fig. 4(c)). The mean size of the kaolin particles was found to be $0.50 \mu\text{m}$ with a standard deviation of $0.17 \mu\text{m}$. From the simulation, it was found that the mean detectable size of the particles that will yield velocity measurements is $0.78 \mu\text{m}$ with a standard deviation of $0.28 \mu\text{m}$. The particle size distribution and detectable particle size distribution along with the sensitivity factors are listed in table II.

Particle Generation System

The kaolin particles were suspended in ethanol and injected into the tunnel using a specialized atomizer system described in reference 6. Two linear arrays of 10 atomizers each were installed on the final set of turning vanes just upstream from the test section. Each pair of adjacent atomizers was controlled by a solenoid valve, which was remotely operated from the control room to allow the desired placement of the particle plume within the test section. The atomizers were spaced on the turning vanes in the manner shown in figure 5 as viewed from the test section. The settling chamber at the location of the turning vanes is 17.68 m in diameter and contracts to 4.85 m at the test section, yielding a contraction ratio of 13.3:1. Since the tunnel flow contains a low-frequency swirl, the plume trajectory cannot be directly estimated from atomizer location and contraction ratio. Therefore the choice of active atomizers was made on the basis of visual sightings of the particles passing through the laser beams and data rate measurements from the high-speed burst counters.

The kaolin particles are irregular in shape with a specific gravity of 2.58 and an index of refraction of 1.56. The aerodynamic particle size analyzer equates the size distribution of the kaolin to the diameter of equivalent spherical particles. The particle size distribution presented in figure 4(a) shows a long trailing

distribution function toward the larger particle sizes. This trailing distribution may be the result of large particles, agglomeration of the smaller particles, or possibly alignment of the irregularly shaped particles with the flow in different orientations. Since the particle size analyzer determines the particle size by measuring the aerodynamic particle response to a known accelerating flow field, the same behavior should be expected within the tunnel flow.

TEST RESULTS

The test consisted of three parts: (1) measurement of free-stream velocity up to Mach 1.0, (2) experimental determination of the sensitivity of the laser velocimeter, and (3) determination of the mean size of the particles detected based on the lag of the particles along the stagnating streamline of the hemisphere model.

Mach Number Test

The traversing mechanism was adjusted to move the laser velocimeter sample volume two model diameters, 38.1 cm, upstream from the model. Two-component velocity measurements were made from Mach 0.1 to Mach 1.0 (results are given in table III). The U-component measurements, illustrated in figure 6, were found to be approximately 1.5 percent below the free-stream velocity calculated from tunnel total temperature, stagnation pressure and Mach number. However, the influence of the model on the flow field can be predicted via the potential flow computer model (ref. 9), and the calculated free-stream velocity adjusted. As illustrated in figure 6(b), the velocity measurements are within the error bands of the tunnel calibration up to a Mach number of 0.5. The remaining measurements were found to be only 0.09 percent above the adjusted free-stream values with a standard deviation of 1.01 percent. The turbulence intensity measured by the laser velocimeter in the U-component, shown in figure 7, is nominally 1 percent over the Mach number range.

The data from the V-component (figs. 8 to 11) indicate a downwash of about 1.25° with peaks occurring at Mach 0.1 and Mach 1.0 of nominally 2.2° . Flow angle is calculated from the mean values of the velocity components (i.e., $\alpha = \arctan \bar{V}/\bar{U}$), since the two components were not coincident (requirement for simultaneous measurements of both velocity components for each particle passage through the sample volume). This procedure does not provide accurate statistics of the flow angle, but does provide an estimate. It is significant that the "turbulence intensity" in the V-component (fig. 9) is large at Mach 0.1, 9.7 percent, and decreases with increasing Mach number until the rise of Mach 1.0. Since a swirl is known to be present in the flow, this apparent "turbulence intensity" may indeed be low-frequency variations in flow angle (fig. 11) and not turbulence. Because the two component measurements were not coincident and thus the cross correlation between the measured velocity components could not be calculated, independence of their variances must be assumed. On the basis of these two assumptions (that the turbulence intensity in the V-component is due to swirl and that the velocity component variances are independent), the standard deviation of the flow angle is large at Mach 0.1 (5.5°) and decreases rapidly to a level of nominally 0.9° until it rises again to 1.3° at Mach 1.0.

Laser Velocimeter Sensitivity and Particle Size Analysis

In the previous section errors due to particle dynamics were not expected since the velocity gradient along the streamline from the point of particle injection to the test section is gradual and theoretical particle dynamics (ref. 10) indicates that particles up to 20 μm in diameter would follow the flow. The flow along the stagnating streamline of a hemisphere however contains severe but known gradients. Particle velocities are predicted to deviate as much as 2.73 m/sec from the expected gas velocity, at $x/D = -0.133$ (the point of maximum deceleration) at Mach 0.8 for particles as small as 1 μm in diameter. Particle velocities were measured from one model diameter upstream, where the mean velocity is nominally 11.5 percent below free-stream conditions due to the presence of the model, to within an estimated distance of 1.9 mm from the model surface for tunnel settings of Mach 0.8 and Mach 1.0. In addition, the velocity flow field was measured at Mach 1.0 at $y/D = -0.533$ since the moderately decelerating flow along this line changes to an accelerating flow as the model is approached until the shock line is reached.

The detailed analysis of the data begins by considering the known test information. From the particle size analysis given previously for the kaolin particles and the predicted sensitivity of the laser velocimeter, the average detectable particle diameter was estimated to be 0.78 μm . The predicted velocity profiles for the three test cases were determined according to the procedure outlined in reference 9 using the tunnel calibration to establish the free-stream conditions. The potential flow method outlined in reference 9 does not include viscous effects, for example, shock wave and boundary layer effects, which are potentially significant at the transonic Mach numbers of 0.8 and 1.0. It is estimated from prior experience that this computational method yields predictions with accuracies on the order of ± 2 percent. The resulting predictions of the gas flow characteristics were used with the particle dynamic prediction procedures from reference 10 to determine the velocities of the average detectable particle, which provide the theoretical reference for comparison with the velocity measurements from the laser velocimeter. The second area of information is that errors in the measurement of cross beam angle yield an unknown bias to the laser velocimeter measurements. The cross beam angle was measured geometrically at a distance of 2.5 m from the sample volume with an estimated uncertainty of ± 1 mm in determining the center of the 13.1-mm-diameter laser beams. This uncertainty yields an unknown bias error in the measurement of the mean velocity within the range of ± 1.45 percent. The final known information is that the model moved downstream during the test because of sting bending, compression of the sting drive gears, etc. This was determined by visually establishing a reference point with the sample volume at the center surface pressure port on the model during setup and finding that the flare that occurs when the sample volume grazes the model was not detected during the test until the laser velocimeter was moved 0.63 mm downstream of the reference point. This distance is not an exact measure of the deflection since flare is detected when the edge of the sample volume (not necessarily the $1/e^2$ intensity location) grazes the model; however it does indicate a movement of the model. The reference point was checked (again visually) following the test and found to repeat.

If the theoretically determined average detectable particle size and the theoretically predicted gas and particle velocity profiles are assumed to be accurate, the bias error in the velocity measurements due to the inaccuracy in the measurement of the cross beam angle may be removed and the actual deflection of the model may be determined. Beginning with the assumption that the model did not move, the least squares errors are determined between the predicted velocity profile for

the average detectable particle size and the measured velocities. Since an inaccuracy in the measurement of the cross beam angle following a system alignment results in an incorrect conversion factor (fringe spacing) from frequency to velocity, the velocity data can be adjusted by multiplying by a correction factor. Through iterative procedures of adjusting the velocity data to minimize the least squares errors between the data and the theoretical velocity profile, the resulting factor can be used to determine the true cross beam angle (within the validity of the assumptions). The theoretical particle velocity profile is then determined for a position downstream to account for the deflection of the model, and the iterative process is repeated. Since the model is known to deflect, a small movement of the velocity profile results in a correction factor closer to 1.0 and a reduction in the least squares errors. Displacement of the velocity profile continues until the minimum least squares error is obtained. Once the minimum least squares error is determined, the particle size is increased and the entire process is repeated until the absolute minimum error is determined. For all three test cases, the minimum error occurred when the particle size was 2.1 μm and the deflection of the model was 1.3 mm downstream. For the Mach 0.8 stagnating streamline case, the cross beam angle was determined to be 3.187° , which represents a bias error of -0.86 percent (an error of 0.6 mm in the measurement of the laser beam separation at the focal distance of 2.5 m). For the Mach 1.0 stagnating streamline case, the cross beam angle was 3.085° (bias error of 2.43 percent), and for the Mach 1.0 $y/D = -0.533$ case, it was 3.158° (bias error of 0.06 percent).

The results for the three test cases are given in table IV and are illustrated in figures 12 to 14. The mean streamwise velocity (\bar{U}) for each measurement ensemble is given along with the mean corrected for cross beam angle measurement error. The differences between the corrected measurements and the predicted particle velocities for a 2.1- μm particle, with the 1.3-mm downstream displacement of the model accounted for, are given in m/sec and percentage of local predicted particle velocity. The average difference was found to be less than 0.05 percent for the three cases indicating the goodness-of-fit of the above procedure with the data.

It was found that the particle trajectory that best fits the measurements is based on a kaolin particle with a diameter of 2.1 μm , whereas the average detectable particle diameter predicted from the aerodynamic particle size analyzer and the laser velocimeter simulation code is 0.78 μm . In an attempt to understand the discrepancy, the sensitivity threshold in the laser velocimeter simulation was raised, since the laser velocimeter characteristics were determined following optimization of the system in the laboratory after the wind tunnel tests were completed and are known not to directly represent the degraded conditions of the system while in the wind tunnel (gradual misalignment due to tunnel vibrations causing a loss in optical system efficiency). This attempt was able to raise the average detectable particle diameter to only 1.4 μm . The effect of the irregularly shaped particles in an optical sense was then determined by measuring the particle size distribution with an optical particle size analyzer (table V and fig. 15). This resulted in a different size distribution from that obtained with the aerodynamic analyzer (table I and fig. 4), which results in a different detectable particle size distribution when multiplied by the laser velocimeter sensitivity function. The calculation of the mean detectable particle size based on the new distribution function yields a particle diameter of 2.33 μm . This indicates that a particle of a single aerodynamic size scatters light at different levels depending on the orientation of the irregularly shaped particle as it passes through the optical size analyzer and likewise through the laser velocimeter sample volume. Therefore

the predicted laser velocimeter sensitivity function, which is calculated based on the assumption of spherical particles, can be used to provide only a rough approximation in this test situation.

As an aid in understanding the aerodynamic process involved in the present situation, consider the effect on the laser velocimeter measurements of the polydisperse particle distribution within the decelerating flow field as a combination of effects from each particle size. If the probability density function of the gas velocity at a location in the decelerating region is represented by figure 16(a), a uniform polydisperse particle size distribution (e.g., seven particle sizes) within the flow would result in the probability density function given in figure 16(b). By considering the polydisperse particle size distribution as being made up of individual particles, one finds that a zero-diameter particle would result in the translation of the velocity distribution (fig. 16(a)) to the left or lowest velocity side of the distribution in figure 16(b). As the particle size increases, the velocity distribution is shifted to the right (higher velocity) because of the lag in the response of the particle to the decelerating flow field. Therefore the resulting probability density function of particle velocity would be determined by a convolution of the probability density function of the gas velocity with the particle velocity lag characteristics as a function of particle size at that point in the flow field. Figure 16(b) shows that for a uniform distribution of particle sizes the center of the velocity probability density function is approximately flat; thus, variations in the center of the density function yield an estimate of the particle size distribution in the flow. Therefore the measured velocity histograms in the decelerating region along the stagnating streamline may be used to estimate the particle size distribution detected by the laser velocimeter within the flow. From this distribution coupled with the particle size distribution measured by the aerodynamic particle size analyzer, the sensitivity function can be estimated. The measured velocity histograms were compared with the velocity trajectories for the particle sizes measured by the aerodynamic analyzer using the histogram divisions from the optical particle size analyzer (table VI and fig. 17). It was found that at x/D of -0.5 and -0.4, there was sufficient spread in velocity due to particle size while the measured local "turbulence intensity" remained low (approximately 2 percent). Assuming that velocities within the histogram below the predicted gas velocity were due to turbulence and removing them along with the corresponding high velocities, the remaining velocity distribution should be due to particle lag differences. Each velocity in the truncated histogram was equated to the particle size required to yield that velocity as predicted by the theoretical particle velocity profiles (fig. 18(c)). The particle size histogram measured by the aerodynamic analyzer (fig. 18(a)) was then divided into the truncated histogram to yield the sensitivity function. It may be seen from figure 18(b) and table VII that the resulting sensitivity function resembles the theoretical sensitivity function in figure 17(b) with the differences found at the extremes most likely from statistical uncertainties due to the low particle count at the corresponding velocities distorting the sensitivity function. The average detectable particle size determined from the truncated histogram was $2.17 \mu\text{m}$ in diameter with a standard deviation of $0.76 \mu\text{m}$.

Since the various sized particles have different velocity profiles, the velocity histogram at each location has a nonzero standard deviation resulting in measurements of turbulence intensity that are larger than the flow turbulence intensity. The standard deviation and apparent turbulence intensity values due to particle lag for the stagnating streamline case at Mach 1.0 are presented in table VIII along with the measured results for the three test cases. The predicted standard deviation is approximately the same (within the statistical accuracy of

the velocity contribution for each of the various particle sizes) as the measured standard deviation. From this comparison, the only estimation that can be made is that the turbulence intensity is low.

The remaining measurement uncertainty is the statistical uncertainty in determining the mean velocity from the measurement ensemble, assuming independence of the individual velocity measurements. This assumption is based on the low data rates obtained during the tunnel tests. These uncertainties are presented in table IX.

CONCLUDING REMARKS

The dedicated laser velocimeter for the Langley 16-Foot Transonic Tunnel has been installed in the tunnel plenum chamber and has operated successfully at Mach numbers from 0.1 to 1.0. Performance tests have shown that the system can measure particle velocities from nominal 2.1- μm -diameter kaolin particles with accuracies of better than 1 percent of the local velocity. The system also satisfies the design specifications of sample volume size, velocity range, and traversing capabilities. Measurement accuracy in flow fields with severe velocity gradients is not within desired specifications because the width of the particle size distribution affects the determination of the mean velocity, since any degradation of the optical system results in rejection of the smaller particles and a corresponding increase in the average detectable particle size. By using particles of constant size, any degradation of the optical system would result in a decrease in measurement rate, but not a decrease in measurement accuracy.

NASA Langley Research Center
Hampton, VA 23665-5225
August 1, 1985

REFERENCES

1. Corson, Blake W., Jr.; Runckel, Jack F.; and Igoe, William B.: Calibration of the Langley 16-Foot Transonic Tunnel With Test Section Air Removal. NASA TR R-423, 1974.
2. Clemmons, James I., Jr.: Laser Velocimeter (Autocovariance) Buffer Interface. NASA TM-83110, 1981.
3. Meyers, James F.; and Walsh, Michael J.: Computer Simulation of a Fringe Type Laser Velocimeter. Proceedings of the Second International Workshop on Laser Velocimetry, Volume I, H. D. Thompson and W. H. Stevenson, eds., Eng. Exp. Stn. Bull. No. 144, Purdue Univ., 1974, pp. 471-510.
4. Mie, G.: Optics of Turbid Media. Ann. Phys., vol. 25, no. 3, Mar. 3, 1908, pp. 377-445.
5. Adrian, Ronald J.; and Earley, Walter L.: Evaluation of LDV Performance Using Mie Scattering Theory. Minnesota Symposium on Laser Anemometry - Proceedings, E. R. G. Eckert, ed., Univ. of Minnesota, Jan. 1976, pp. 426-454.
6. Reubush, D. E.; and Franke, J. M.: Some Solutions to the Problems and Pitfalls of Laser Velocimetry in a Large Transonic Wind Tunnel. Engineering Applications of Laser Velocimetry, Hugh W. Coleman and Philip A. Pfund, eds., American Soc. Mech. Eng., c.1982, pp. 7-12.
7. Remiarz, R. J.; Agarwal, J. K.; Quant, F. R.; and Sem, G. J.: Real-Time Aerodynamic Particle Size Analyzer. Aerosols in the Mining and Industrial Work Environments, Virgil A. Marple and Benjamin Y. H. Liu, eds., Ann Arbor Science, 1983, pp. 879-895.
8. Sem, Gilmore J.: Aerodynamic Particle Size: Why Is It Important? TSI Q., vol. X, issue 3, July-Sept. 1984, pp. 3-12.
9. Reyhner, Theodore A.: Computation of Transonic Potential Flow About Three-Dimensional Inlets, Ducts, and Bodies. NASA CR-3514, 1982.
10. Walsh, Michael J.: Influence of Particle Drag Coefficient on Particle Motion in High-Speed Flow With Typical Laser Velocimeter Applications. NASA TN D-8120, 1976.

TABLE I.- SYSTEM CHARACTERISTICS OF THE DEDICATED LASER VELOCIMETER
FOR THE 16-FOOT TRANSONIC TUNNEL (U-COMPONENT)

[The characteristics of the V-component are the same as the U-component]
except the laser wavelength is 488.0 nm

Laser wavelength, nm	514.5
Input lens focal length, m	2.74
Input laser power, W	1.8
Diameter of laser beam at input lens, mm	7.5
Cross beam angle, deg	3.16
Beam A:	
Position (x,y), m	-0.076, 0
Polarization, deg	93.0
Transmission coefficient	0.2
Beam B:	
Position (x,y), m	0.076, 0
Polarization, deg	103.0
Transmission coefficient	0.31
Receiver:	
Lens focal length, m	2.74
Horizontal rotation angle, deg	180.0
Vertical rotation angle, deg	0.0
Effective lens diameter, m	0.165
Transmission coefficient	0.474
Electronics:	
Photomultiplier quantum efficiency	0.21
Photomultiplier gain	8.75×10^6
Low-pass filter cutoff, MHz	64.0
High-pass filter cutoff, MHz	32.0
Counter threshold voltage, V	0.05
Counter count comparison accuracy	0.02
Sample volume characteristics:	
Diameter, mm	0.31
Length, mm	6.1
Fringe spacing, μ m	9.33

TABLE II.- KAOLIN PARTICLE SIZE DISTRIBUTION DETERMINED BY THE
AERODYNAMIC PARTICLE SIZE ANALYZER, THEORETICAL LV
MEASUREMENT SENSITIVITY, AND DETECTABLE PARTICLE
SIZE DISTRIBUTION

Particle diameter, μm	Fraction of total particles, percent	LV sensitivity factor	Fraction of detectable particles, percent
0.30	4.72	0	0
.31	1.91	0	0
.34	3.12	0	0
.36	8.28	0	0
.39	13.90	0	0
.42	12.43	0	0
.45	10.75	0	0
.48	9.43	0.07	4.28
.52	7.74	.41	19.93
.56	6.06	.06	2.33
.60	5.22	0	0
.64	4.09	.48	12.49
.69	3.14	.58	11.50
.74	2.61	.34	5.55
.80	1.84	.89	10.37
.86	1.39	.79	6.93
.92	1.05	1.11	7.40
.99	.73	1.04	4.77
1.06	.51	1.29	4.14
1.15	.35	1.43	3.20
1.23	.26	1.17	1.91
1.32	.17	1.76	1.85
1.42	.10	1.76	1.13
1.53	.06	1.82	.73
1.64	.04	1.84	.50
1.76	.03	1.83	.33
1.90	.02	1.66	.20
2.04	.01	1.79	.15
2.19	.01	1.24	.07
2.35	.01	1.18	.06
2.53	.01	1.44	.05
2.72	0	1.02	.03
2.92	0	1.76	.04
3.14	0	1.78	.02
3.37	0	1.76	.02
3.62	0	.81	.01
3.90	0	1.69	.01
4.19	0	1.13	.01
4.50	0	1.72	.01
4.84	0	1.34	0

^aEquivalent physical size assuming spherical particles.

TABLE III.- VELOCITY AND FLOW ANGLE MEASUREMENTS AT $x/D = -2.0$
AS A FUNCTION OF MACH NUMBER

M	\bar{U}_{meas} , m/sec	\bar{U}_{gas} , m/sec (a)	Uncertainty in \bar{U}_{gas} , m/sec	Difference, percent	$\sigma_{U,\text{meas}}$, m/sec	$(\sigma_U/\bar{U})_{\text{meas}}$, percent	$\sigma_{U,\text{corr}}$, m/sec (b)	$(\sigma_U/\bar{U})_{\text{corr}}$, percent (b)
0.1	34.6	33	± 3.2	0	0.26	0.75	0.26	0.75
.2	65.6	65	± 1.6	0	.52	.79	.52	.79
.2	65.5	65	± 1.6	0	.49	.75	.49	.75
.2	65.8	65	± 1.6	0	.51	.78	.51	.78
.3	97.9	97	± 1.1	0	.87	.89	.86	.89
.3	97.8	97	± 1.1	0	.88	.90	.88	.90
.4	129	129	$\pm .8$	0	1.17	.91	1.16	.91
.5	162	161	$\pm .7$	0.2	1.36	.84	1.34	.83
.6	194	192	$\pm .6$.7	2.30	1.19	2.28	1.18
.7	225	223	$\pm .6$.6	2.47	1.10	2.44	1.07
.8	254	253	$\pm .6$.2	2.76	1.09	2.72	1.07
.8	256	253	$\pm .6$.9	2.90	1.13	2.86	1.11
.9	284	283	$\pm .6$.1	3.32	1.17	3.26	1.14
1.0	305	312	$\pm .6$	-2.1	3.15	1.03	3.07	1.00

M	\bar{U}_{meas} , m/sec	\bar{V}_{meas} , m/sec	$\sigma_{V,\text{meas}}$, m/sec	$(\sigma_V/\bar{U})_{\text{meas}}$, percent	$(\sigma_V/\bar{U})_{\text{corr}}$, percent (b)	$\bar{\alpha}_{\text{meas}}$, deg	$\sigma_{\alpha,\text{corr}}$, deg (b)
0.1	34.6	-1.31	3.50	10.09	9.67	-2.16	5.52
.2	65.6	-.84	3.44	5.24	5.00	-.74	2.86
.2	65.5	-1.21	3.69	5.63	5.41	-1.06	3.10
.2	65.8	-1.98	3.93	5.97	5.78	-1.72	3.31
.3	97.9	-1.99	3.29	3.36	3.20	-1.16	1.83
.3	97.8	-1.90	3.07	3.14	2.96	-1.11	1.70
.4	129	-2.27	3.33	2.58	2.45	-1.01	1.41
.5	162	-3.30	3.00	1.85	1.75	-1.17	1.00
.6	194	-4.03	2.99	1.54	1.46	-1.19	.83
.7	225	-3.95	3.78	1.68	1.62	-1.01	.93
.8	254	-6.44	3.45	1.36	1.30	-1.45	.74
.8	256	-3.67	4.55	1.78	1.74	-.82	1.00
.9	284	-6.02	3.64	1.28	1.23	-1.21	.71
1.0	305	-11.91	7.22	2.37	2.34	-2.23	1.34

^aTheoretical gas velocity, calculated from free-stream tunnel conditions, has been adjusted for the presence of the model.

^bMeasured standard deviation corrected for counter quantizing error.

TABLE IV.—CORRECTED U-COMPONENT VELOCITY MEASUREMENTS AND COMPARISONS WITH THE THEORETICALLY PREDICTED VELOCITY PROFILES FOR A 2.1- μ M DIAMETER KAOLIN PARTICLE

mean streamwise velocity corrected for cross beam angle measurement errors.

TABLE V.- KAOLIN PARTICLE SIZE DISTRIBUTION DETERMINED BY THE
OPTICAL PARTICLE SIZE ANALYZER, THEORETICAL LV MEASUREMENT
SENSITIVITY, AND DETECTABLE PARTICLE SIZE DISTRIBUTION

Particle diameter, μm	Fraction of total particles, percent	LV sensitivity factor	Fraction of detectable particles, percent
0.25	2.61	0	0
.39	17.15	0	0
.68	10.64	.59	5.79
.95	9.74	1.13	10.22
1.20	7.80	1.44	10.44
1.44	6.41	1.73	10.32
1.66	5.56	1.80	9.31
1.89	4.61	1.58	6.78
2.10	4.16	1.70	6.57
2.32	3.48	1.45	4.70
2.52	3.16	2.20	6.46
2.73	2.81	1.21	3.15
2.93	2.45	1.55	3.54
3.12	2.15	1.83	3.67
3.32	2.06	0	0
3.51	1.77	1.25	2.05
3.70	1.59	0	0
3.89	1.52	1.28	1.81
4.07	1.32	0	0
4.26	1.18	1.59	1.75
4.44	1.12	1.84	1.92
4.62	.91	1.39	1.17
4.80	.87	2.36	1.91
4.97	.71	1.69	1.12
5.15	.70	2.37	1.53
5.32	.58	1.93	1.05
5.49	.49	1.93	.89
5.67	.45	2.10	.88
5.84	.41	1.45	.55
6.01	.34	1.83	.57
6.17	.24	2.10	.47
6.34	.24	1.44	.33
6.51	.22	2.03	.42
6.67	.20	0	0
6.84	.15	1.90	.26
7.00	.12	1.77	.21
7.16	.05	2.37	.11
7.32	.03	2.17	.05
7.48	0	2.24	0
7.64	0	2.62	0
7.80	0	2.35	0

^aEquivalent physical size assuming spherical particles.

TABLE VI.- KAOLIN PARTICLE SIZE DISTRIBUTION DETERMINED BY THE
 AERODYNAMIC PARTICLE SIZE ANALYZER (ADJUSTED TO MATCH
 PARTICLE SIZE DIVISIONS IN THE OPTICAL SIZE ANALYZER),
 THEORETICAL LV MEASUREMENT SENSITIVITY, AND DETECTABLE
 PARTICLE SIZE DISTRIBUTION

Particle diameter, μm	Fraction of total particles, percent	LV sensitivity factor	Fraction of detectable particles, percent
0.25	4.29	0	0
.39	48.05	0	0
.68	24.48	.59	30.97
.95	9.69	1.13	23.60
1.20	4.73	1.44	14.72
1.44	2.63	1.73	9.85
1.66	1.67	1.80	6.50
1.89	1.12	1.58	3.82
2.10	.80	1.70	2.94
2.32	.57	1.45	1.78
2.52	.45	2.20	2.12
2.73	.33	1.21	.85
2.93	.27	1.55	.90
3.12	.22	1.83	.87
3.32	.16	0	0
3.51	.15	1.25	.40
3.70	.13	0	0
3.89	.09	1.28	.23
4.07	.07	0	0
4.26	.06	1.59	.21
4.44	.06	1.84	.23

^aEquivalent physical size assuming spherical particles.

TABLE VII.- KAOLIN PARTICLE SIZE DISTRIBUTION DETERMINED BY THE
 AERODYNAMIC PARTICLE SIZE ANALYZER, ESTIMATED DETECTABLE
 PARTICLE SIZE DISTRIBUTION, AND LV ESTIMATED
 MEASUREMENT SENSITIVITY FUNCTION

Particle diameter, μm	Fraction of total particles, percent	Estimated LV sensitivity factor ^b	Estimated fraction of detectable particles, ^c percent
0.25	4.29	0.01	0.49
.39	48.05	0	.49
.68	24.48	.01	1.85
.95	9.69	.04	3.95
1.20	4.73	.09	4.07
1.44	2.63	.35	9.26
1.66	1.67	.61	10.25
1.89	1.12	1.02	11.48
2.10	.80	1.47	11.73
2.32	.57	2.22	12.59
2.52	.45	2.38	10.62
2.73	.33	1.62	5.31
2.93	.27	2.12	5.68
3.12	.22	1.00	2.22
3.32	.16	2.40	3.83
3.51	.15	1.00	1.48
3.70	.13	1.56	2.10
3.89	.09	1.16	.99
4.07	.07	.90	.62
4.26	.06	.82	.49
4.44	.06	.22	.12

^aEquivalent physical size assuming spherical particles.
 Particle size divisions adjusted to match those of optical analyzer.

^bObtained by dividing estimated detectable particle size distribution by particle size distribution.

^cEstimated from velocity histograms at $x/D = -0.5$ and -0.4 at Mach 1.0.

TABLE VIII--MEASURED STANDARD DEVIATIONS AND TURBULENCE INTENSITIES FOR U-COMPONENT AND A COMPARISON OF THE RESULTS AT MACH 1.0 WITH THE THEORETICAL VALUES

Mach 0.8 Stagnating streamline		Mach 1.0 Stagnating streamline				Mach 1.0 Y/D = -0.533		
x/D	$\sigma_{U,meas}'$ (\bar{U}) meas' m/sec	x/D	$\sigma_{U,meas}'$ (\bar{U}) meas' m/sec	$\sigma_{U,part}'$ (\bar{U}) part' m/sec (a)	$\sigma_{U,part}'$ (\bar{U}) part' percent (a)	x/D	$\sigma_{U,meas}'$ m/sec	(σ_{U}/\bar{U}) meas' percent
-2.0	3.07	1.17	-2.0	3.15	1.04	0	0	1.43
-1.5	2.82	1.10	-1.5	3.14	1.03	.95	-1.5	1.19
-1.0	2.86	1.15	-1.0	3.88	1.34	1.89	.65	1.39
-0.5	3.88	1.77	-.5	4.50	1.82	4.27	1.72	1.11
-.47	3.27	1.51	-.4	4.50	1.96	5.26	2.27	1.51
-.4	4.12	2.01	-.4	5.87	2.56	5.26	2.27	1.75
-.3	4.269	2.50	-.3	8.56	4.13	6.49	3.12	4.32
-.3	7.37	3.94	-.2	5.72	3.34	8.01	4.58	3.85
-.2	5.73	3.62	-.1	8.50	7.01	9.52	7.82	4.10
-.2	7.11	4.47	-.08	8.33	7.89	9.75	9.10	4.32
-1	6.62	6.18	-.06	8.94	10.28	9.91	10.96	3.13
-.08	7.00	7.53	-.04	8.68	12.38	9.91	13.98	1.33
-.06	8.44	10.69	-.02	8.44	19.20	9.58	20.07	6.16
-.04	7.77	13.00	-.013	9.81	27.29	9.03	23.80	2.57
-.02	8.49	20.64	-.0067	6.84	28.90	8.41	29.59	2.40
-.02	10.41	26.49	-.0033	6.81	35.16	8.04	34.98	6.22
-.013	8.26	21.49						
-.0067	6.43	29.70						
-.0033	6.98	42.52						

^aDetermined from velocity differences due to particle dynamics and from the particle size distribution.

TABLE IX.- STATISTICAL UNCERTAINTY IN THE MEASURED MEAN U-COMPONENT

Mach 0.8 Stagnating streamline				Mach 1.0 Stagnating streamline				Mach 1.0 Y/D = -0.533			
x/D	\bar{U} , m/sec	Uncertainty in \bar{U}		x/D	\bar{U} , m/sec	Uncertainty in \bar{U}		x/D	\bar{U} , m/sec	Uncertainty in \bar{U}	
		m/sec	percent			m/sec	percent			m/sec	percent
-2.0	260.4	±0.24	±0.09	-2.0	313	±0.21	±0.07	-2.0	316	±0.50	±0.16
-1.5	257.0	±.17	±.07	-1.5	304	±.20	±.06	-1.5	309	±.42	±.14
-1.0	248.6	±.19	±.08	-1.0	290	±.26	±.09	-1.0	295	±.47	±.16
-.5	219.5	±.23	±.10	-.5	247	±.27	±.11	-.5	263	±.30	±.12
-.47	216.5	±.16	±.08	-.4	230	±.39	±.17	-.4	256	±.46	±.18
-.4	205.5	±.59	±.31	-.4	229	±.28	±.13	-.3	246	±.51	±.21
-.3	187.6	±1.47	±.78	-.3	207	±1.68	±.82	-.2	237	±.36	±.15
-.3	187.4	±.79	±.50	-.2	171	±1.38	±.77	-.133	232	±.33	±.41
-.2	158.0	±2.05	±1.28	-.1	121	±.90	±.75	-.067	228	±.47	±.21
-.2	158.6	±.37	±.17	-.08	106	±.83	±.80	0	227	±.34	±.15
-.1	107.3	±.80	±.73	-.06	86.9	±.81	±.95	.067	230	±.69	±.30
-.08	93.2	±.73	±.78	-.04	70.1	±1.01	±1.46	.133	239	±.92	±.39
-.06	79.1	±.81	±1.02	-.02	44.0	±.87	±2.03	.2	259	±1.07	±.42
-.4	59.8	±.72	±1.20	-.013	35.9	±1.20	±3.39				
-.02	41.0	±.76	±1.83	-.0067	23.7	±.69	±2.96				
-.02	39.3	±.81	±2.05	-.0033	19.4	±.67	±3.53				
-.02	39.8	±.48	±1.19								
-.013	30.6	±.43	±1.39								
-.0067	21.6	±.39	±1.79								
-.0033	16.4	±.41	±2.51								
Average . . .		±0.77	±1.15	Average . . .		±1.17	±1.56	Average . . .		±0.57	±0.23

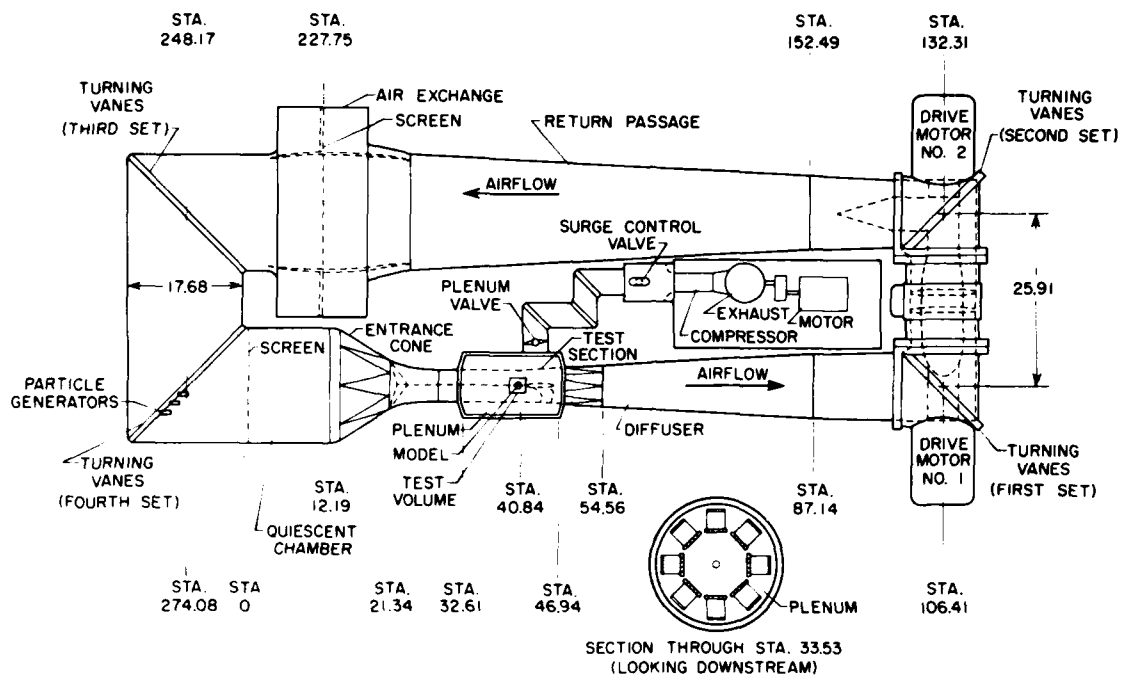


Figure 1.- Schematic of the Langley 16-Foot Transonic Tunnel. (Dimensions are in meters.)



Figure 2.- Hemisphere-cylinder model in the Langley 16-Foot Transonic Tunnel.

L84-1994

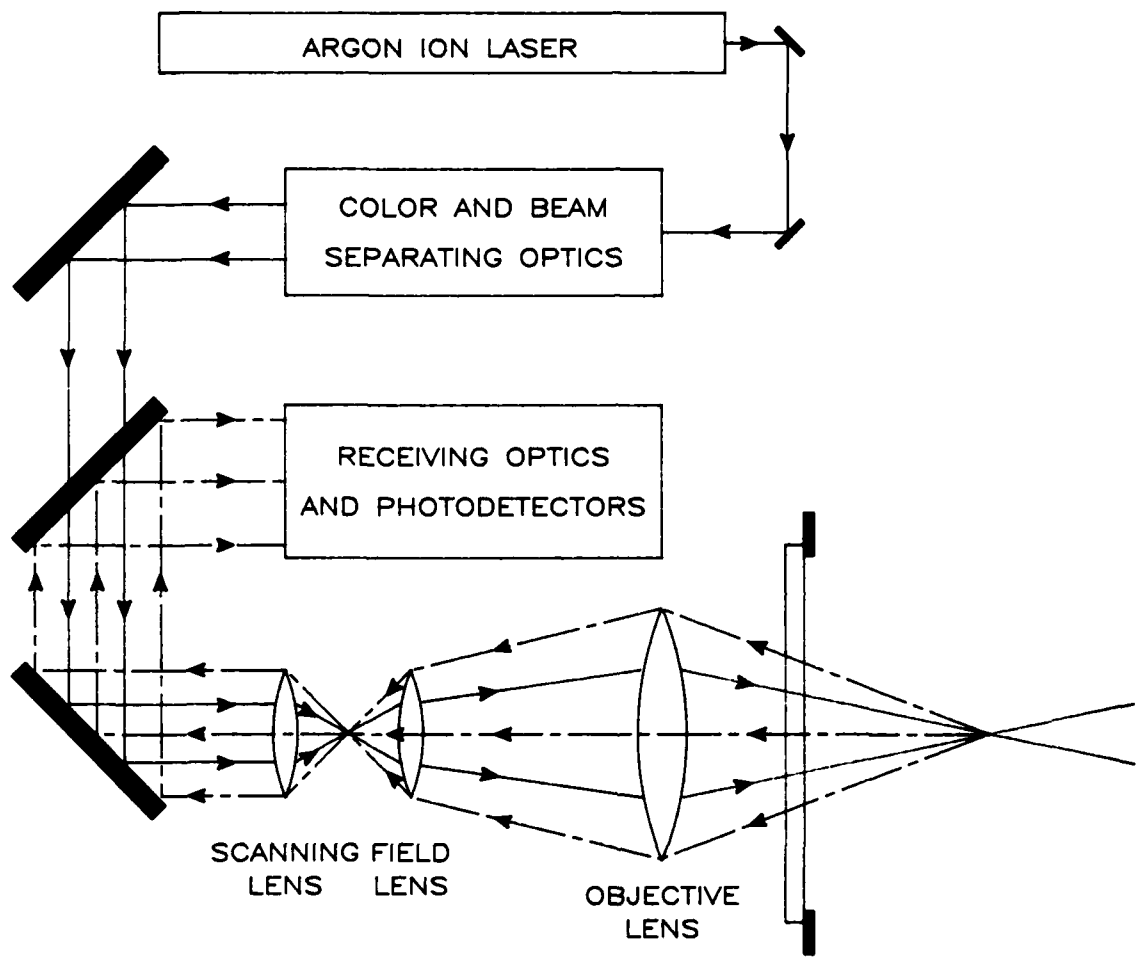
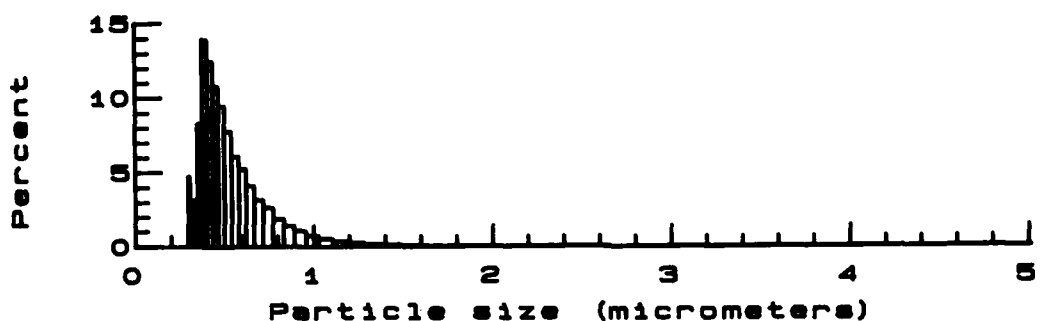
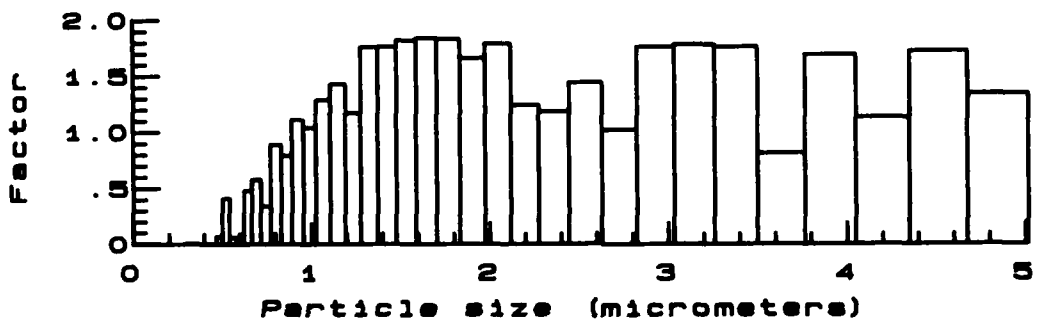


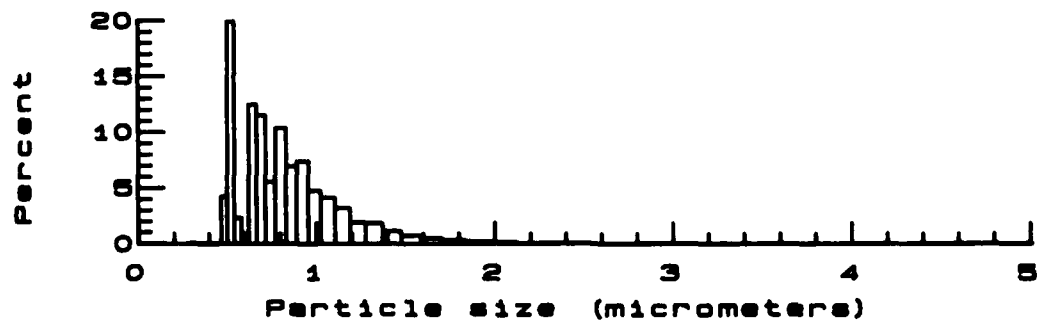
Figure 3.- Block diagram of laser velocimeter optical system.



(a) Particle size distribution.



(b) LV sensitivity factors.



(c) Detectable particle size distribution.

Figure 4.- Kaolin particle size distribution determined by aerodynamic particle size analyzer, theoretical LV measurement sensitivity, and detectable particle size distribution.

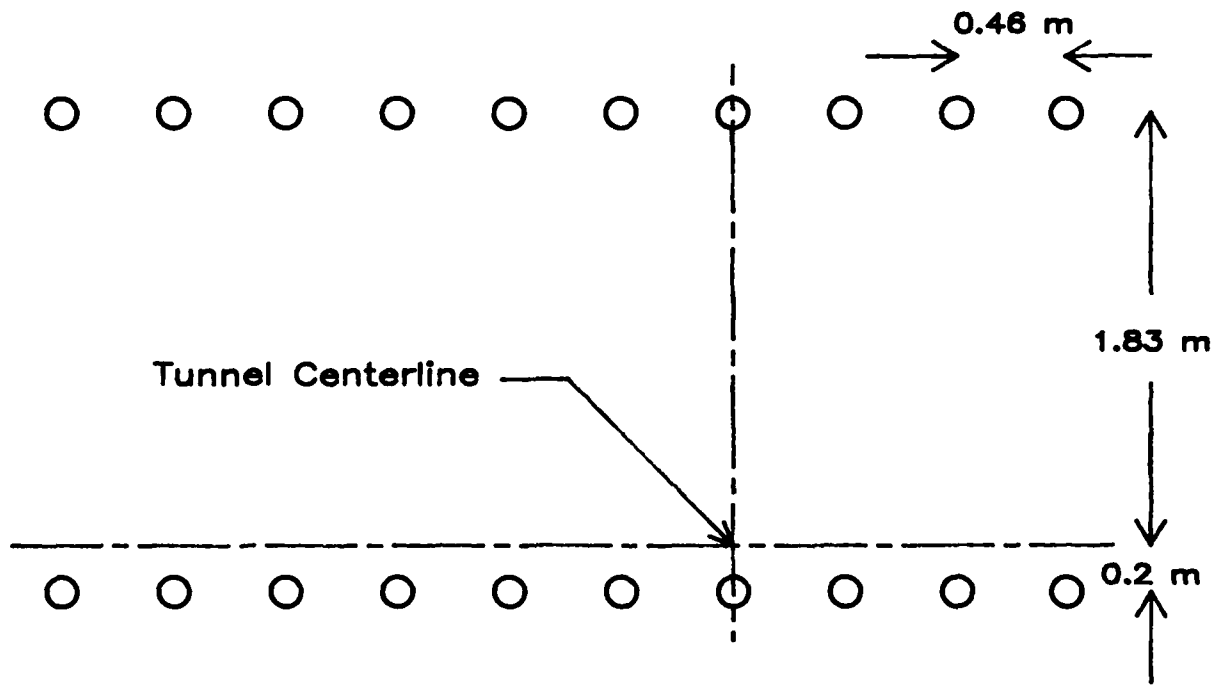
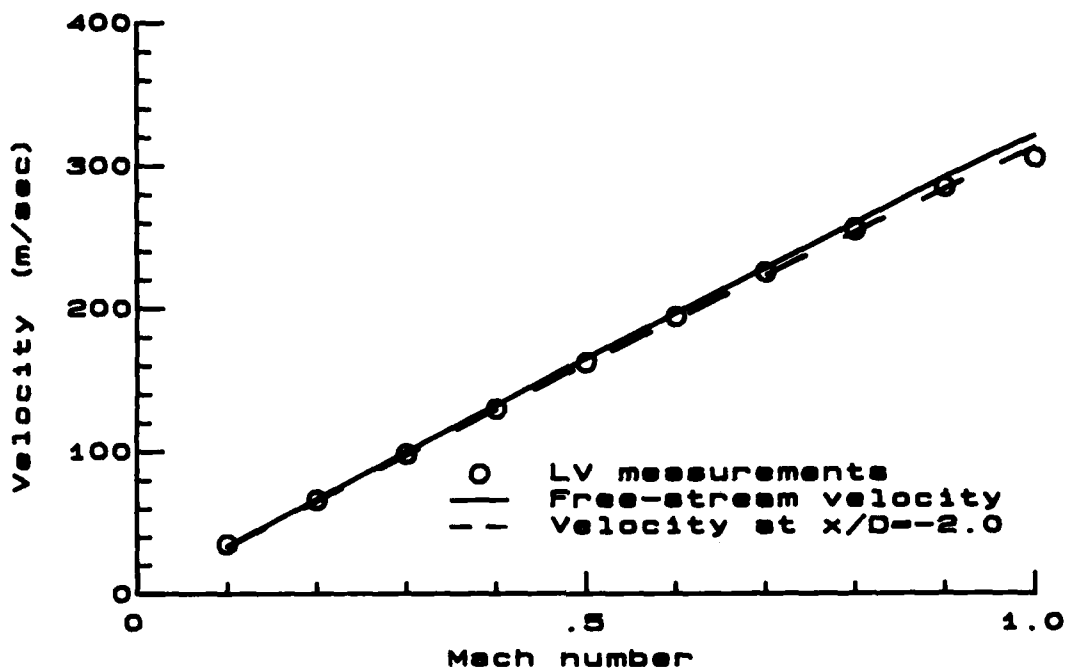
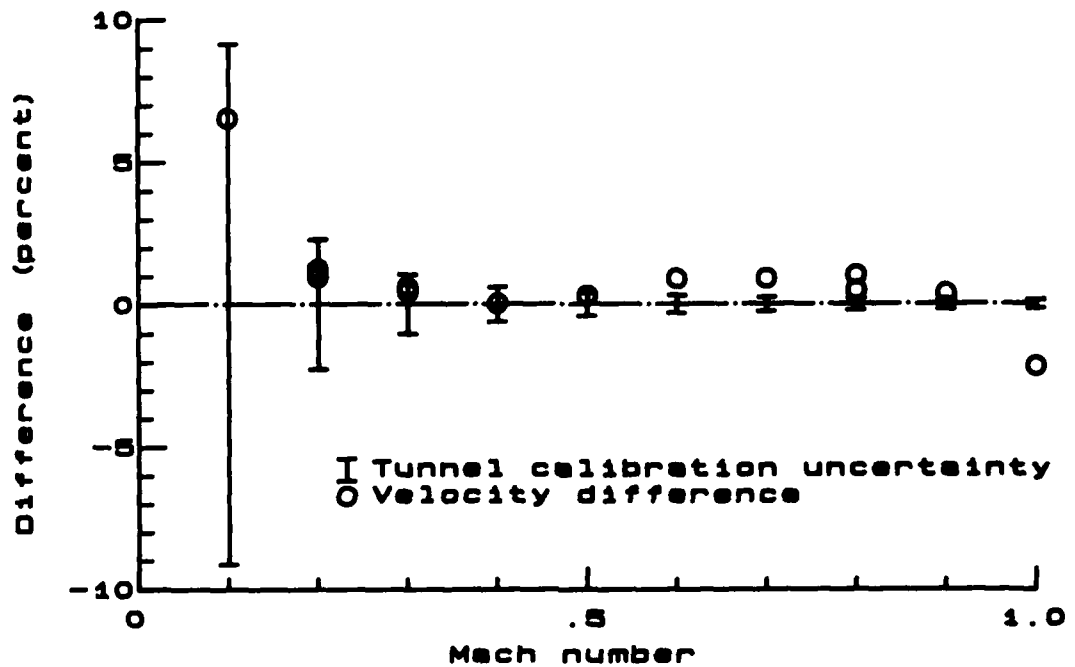


Figure 5.- Placement of particle generators in settling chamber.
Viewed from the test section.



(a) Measured and calculated velocities.



(b) Difference between the measured velocity and calculated tunnel velocity. Difference = $(U_{\text{meas}} - U_{\text{gas}})/U_{\text{gas}}$.

Figure 6.- Measured mean U-component as a function of Mach number and comparison with calculated tunnel velocity. $x/D = -2.0$.

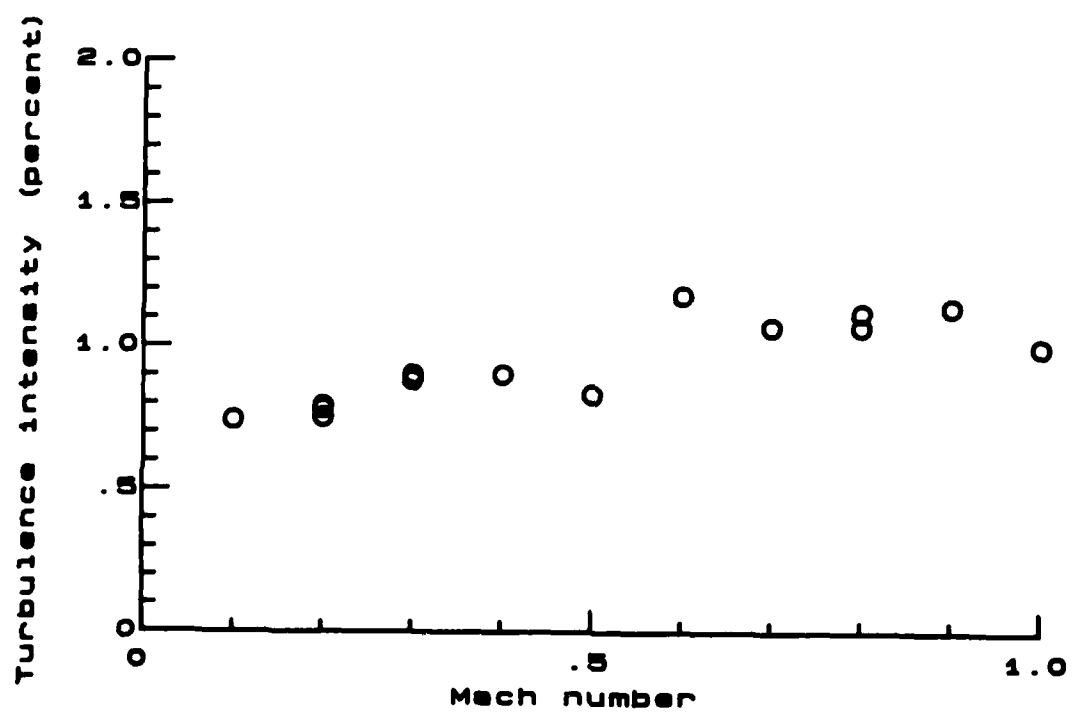


Figure 7.- Corrected turbulence intensity measurements for U-component as a function of Mach number. $x/D = -2.0$.

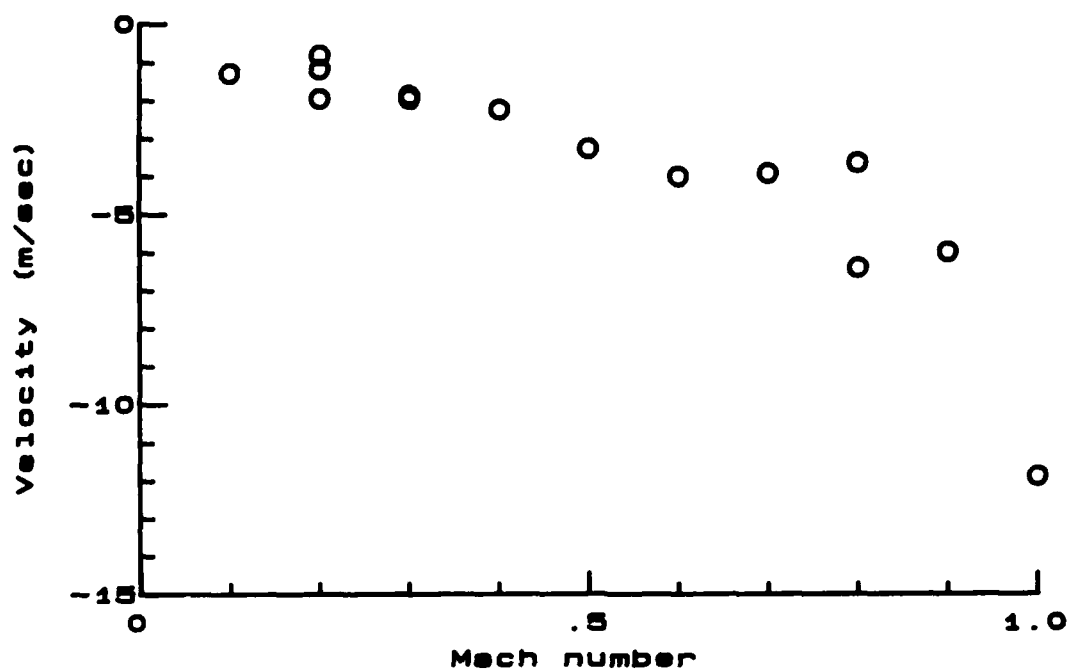


Figure 8.- Measured mean V-component as a function of Mach number.
 $x/D = -2.0$.

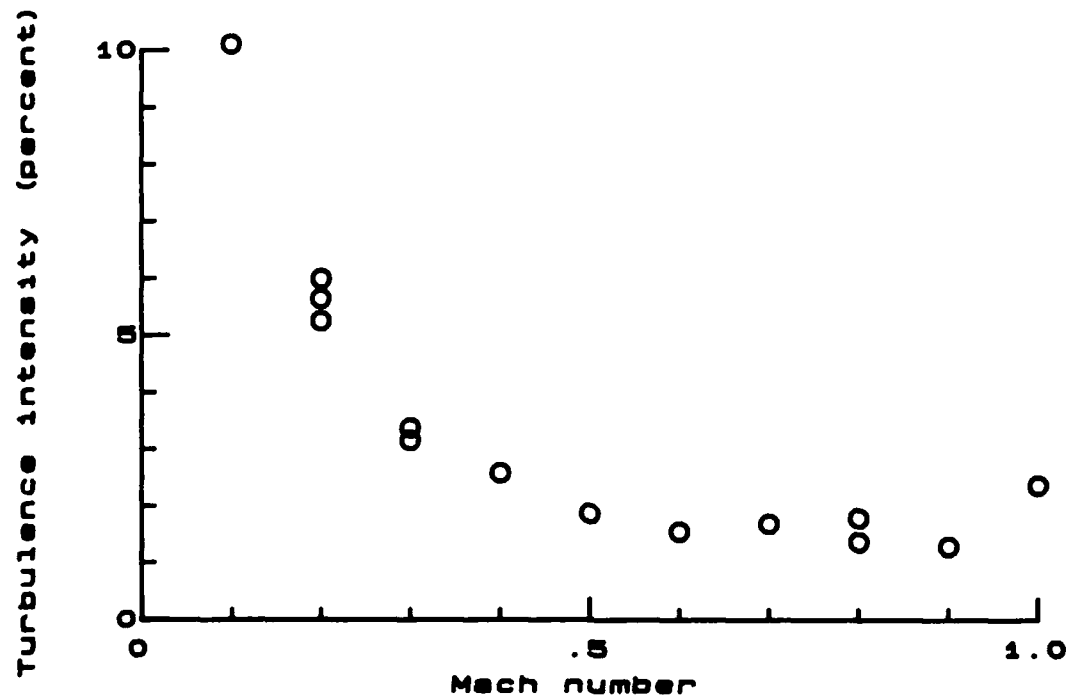


Figure 9.- Corrected turbulence intensity measurements for V-component as a function of Mach number. $x/D = -2.0$.

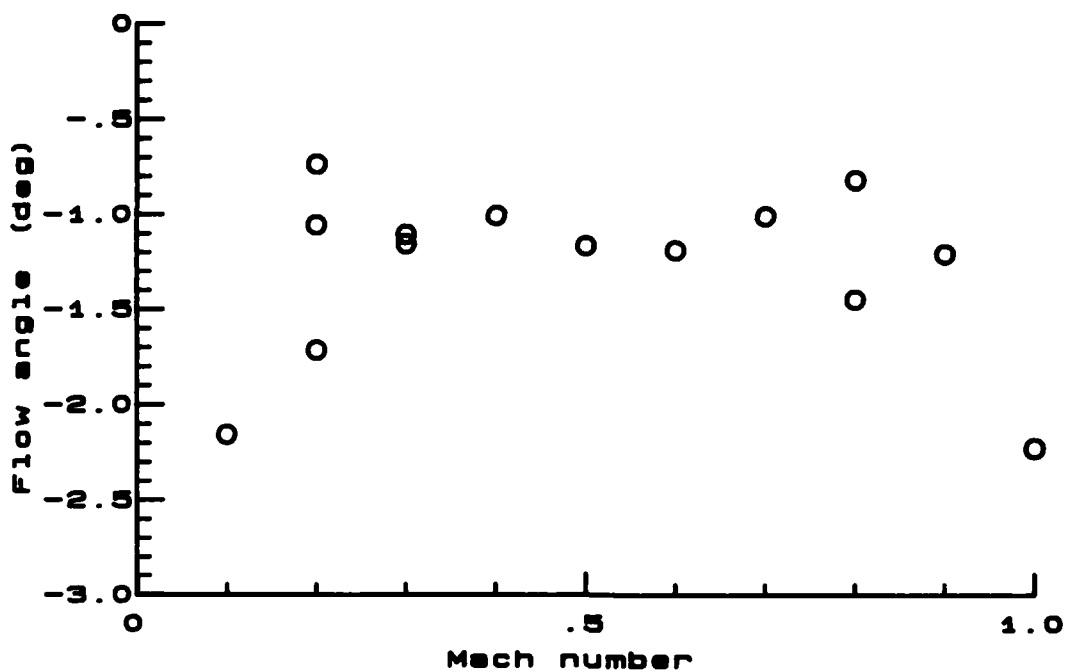


Figure 10.- Measured mean flow angle (UV-plane) as a function of Mach number. $x/D = -2.0$.

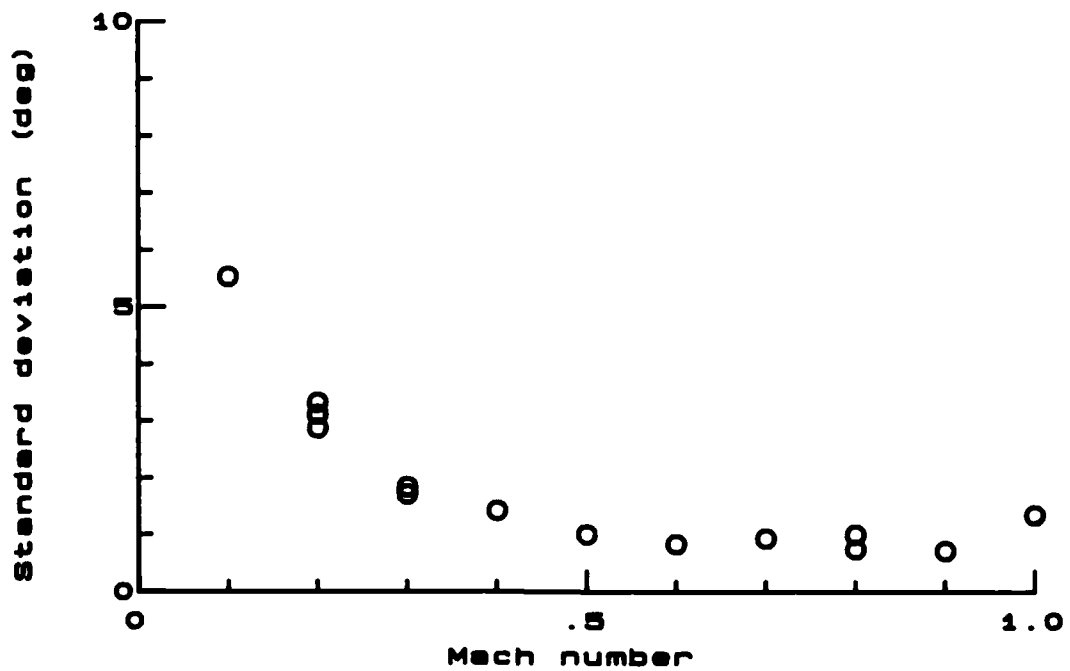
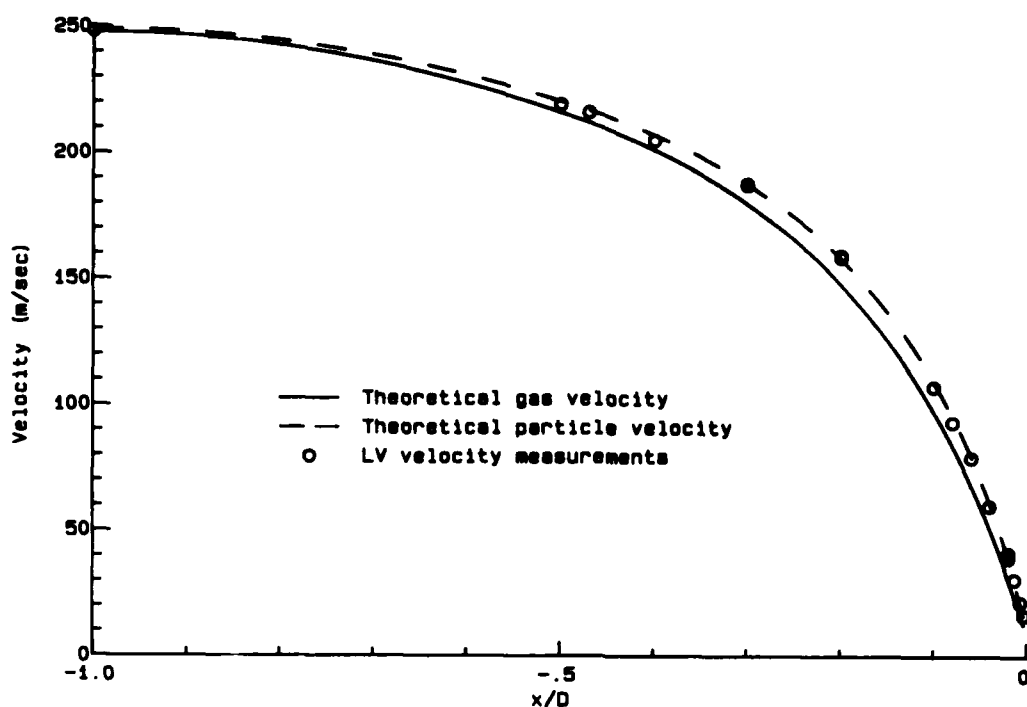
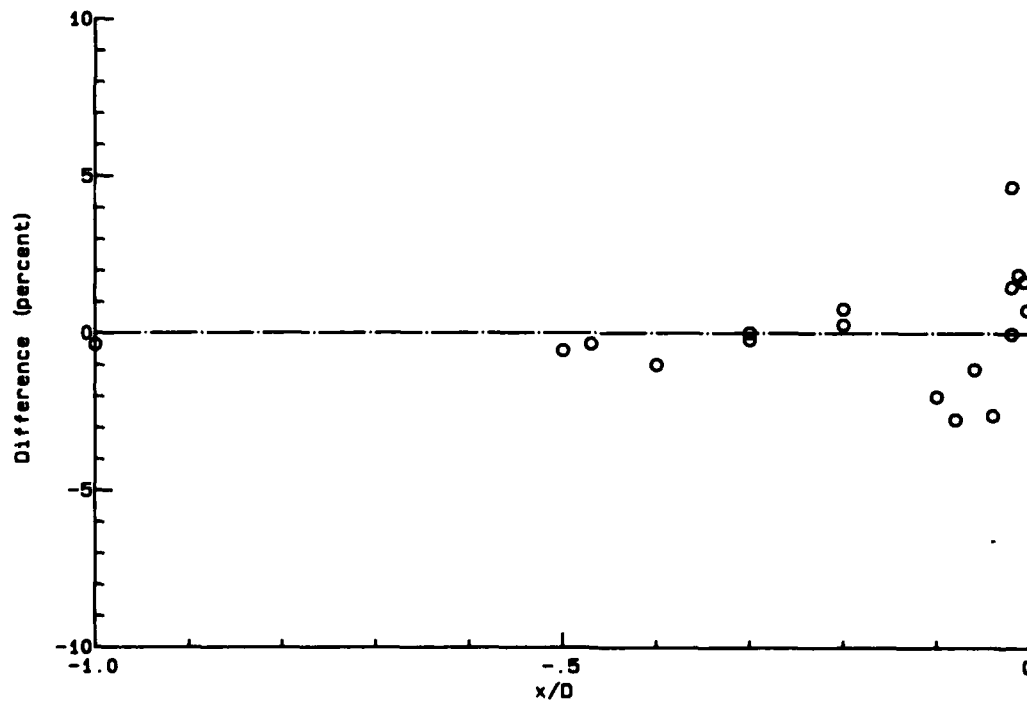


Figure 11.- Standard deviation of flow angle (UV-plane) as a function of Mach number. $x/D = -2.0$.



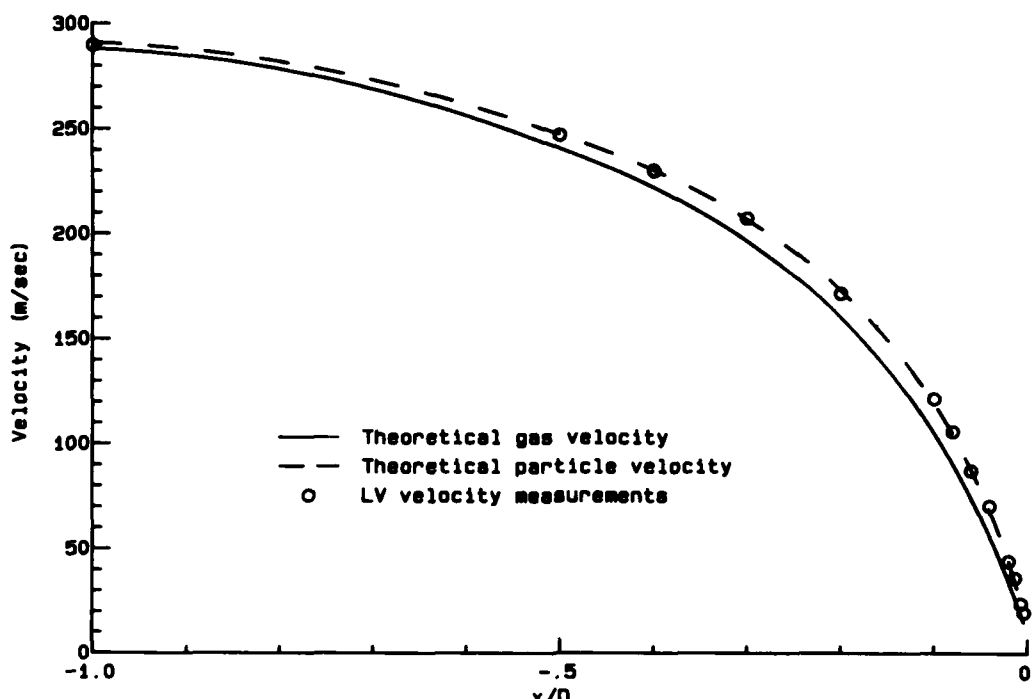
(a) Measured and predicted velocities.



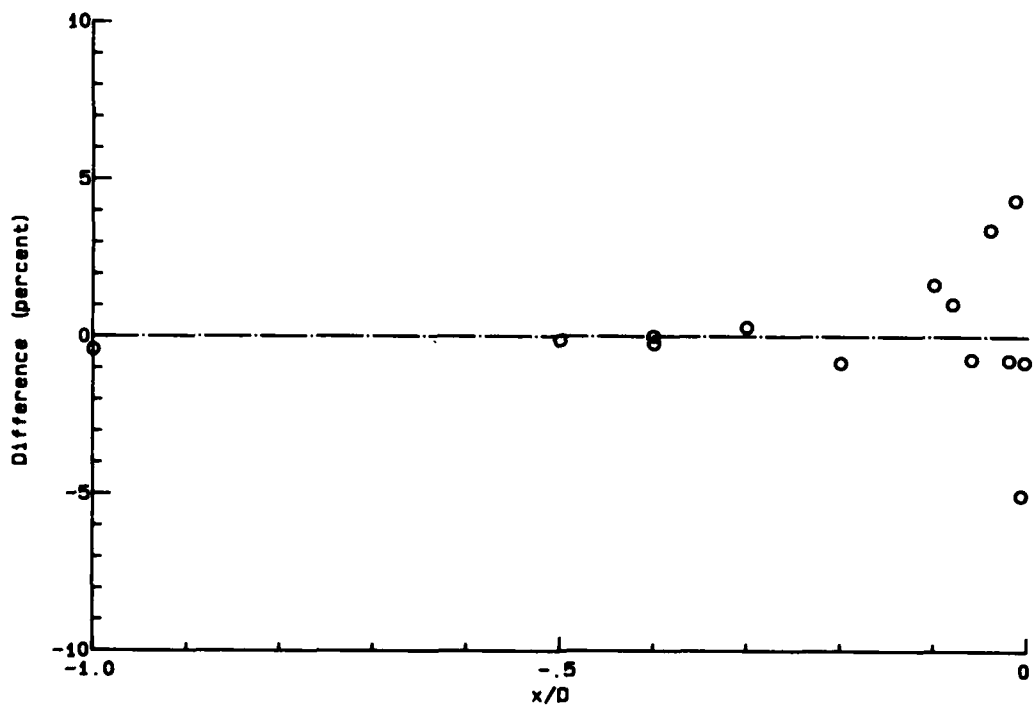
(b) Difference between measured and predicted velocities.

$$\text{Difference} = (\bar{U}_{\text{meas}} - \bar{U}_{\text{part}}) / \bar{U}_{\text{part}}$$

Figure 12.- Measured mean U-component along stagnating streamline of hemisphere-cylinder model at Mach 0.8 and comparison with theoretical particle velocity.



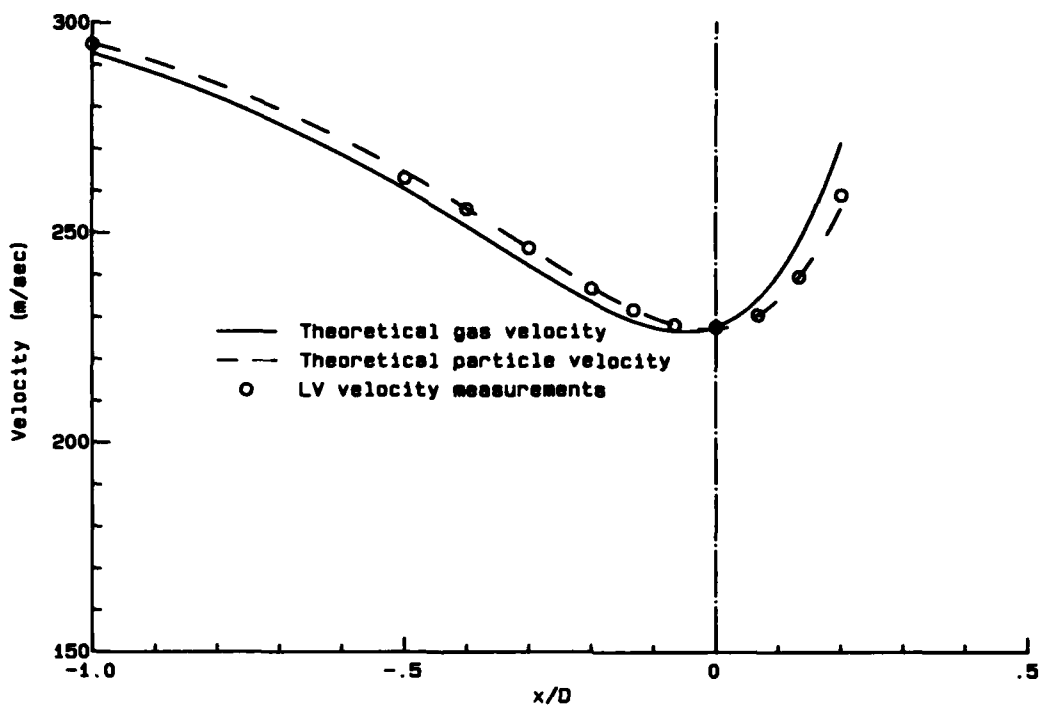
(a) Measured and predicted velocities.



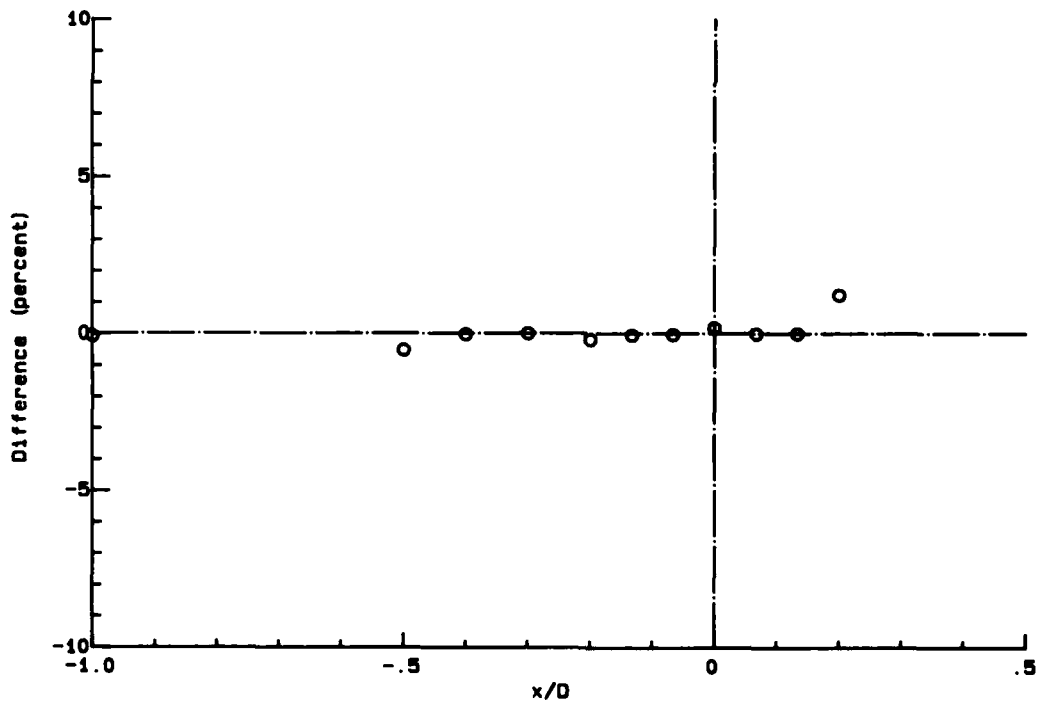
(b) Difference between measured and predicted velocities.

$$\text{Difference} = (\bar{U}_{\text{meas}} - \bar{U}_{\text{part}}) / \bar{U}_{\text{part}}$$

Figure 13.- Measured mean U-component along stagnating streamline of hemisphere-cylinder model at Mach 1.0 and comparison with theoretical particle velocity.



(a) Measured and predicted velocities.



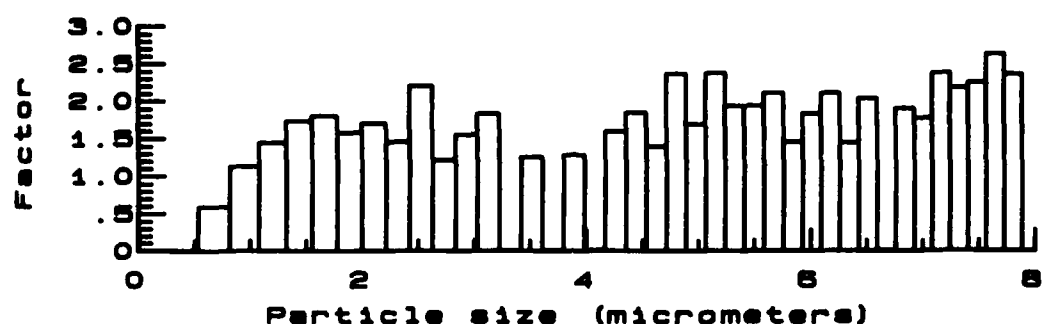
(b) Difference between measured and predicted velocities.

$$\text{Difference} = (\bar{U}_{\text{meas}} - \bar{U}_{\text{part}}) / \bar{U}_{\text{part}}$$

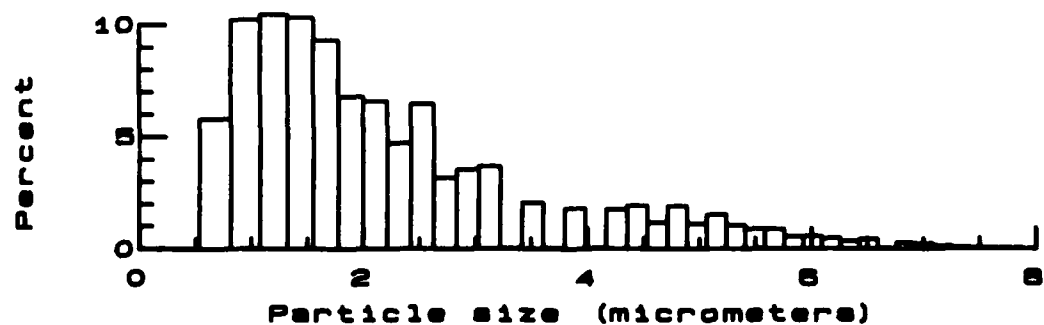
Figure 14.- Measured mean U-component along $y/D = -0.533$ at Mach 1.0.



(a) Particle size distribution.

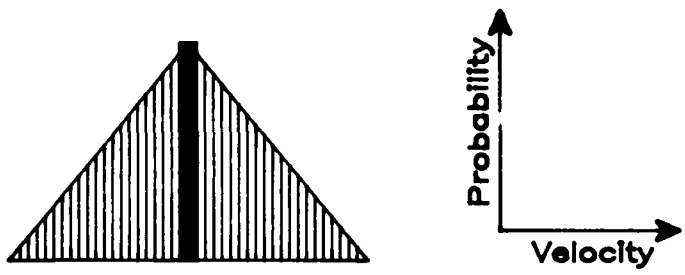


(b) LV sensitivity factors.

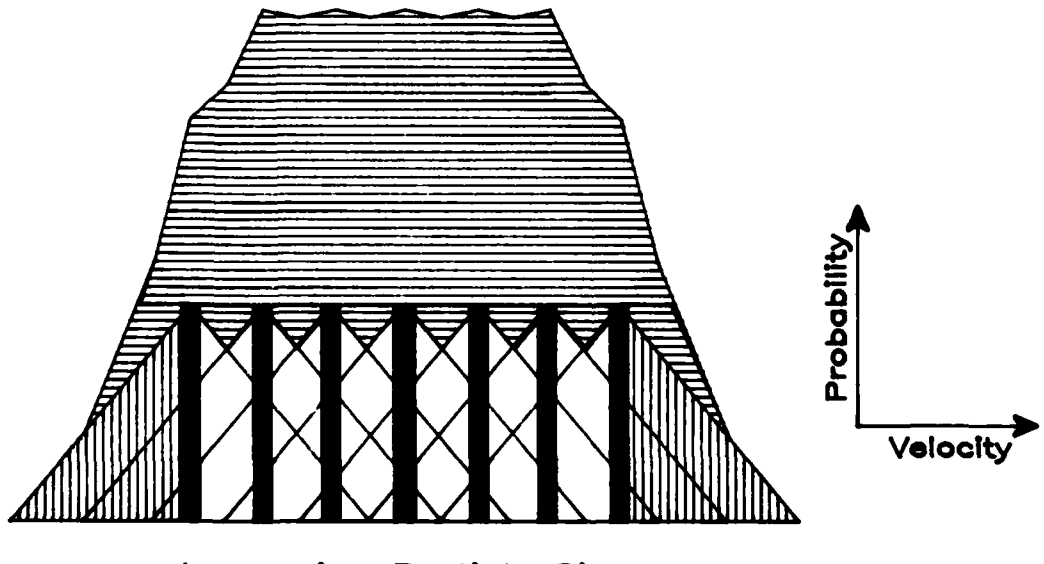


(c) Detectable particle size distribution.

Figure 15.- Kaolin particle size distribution determined by optical particle size analyzer, theoretical LV measurement sensitivity, and detectable particle size distribution.

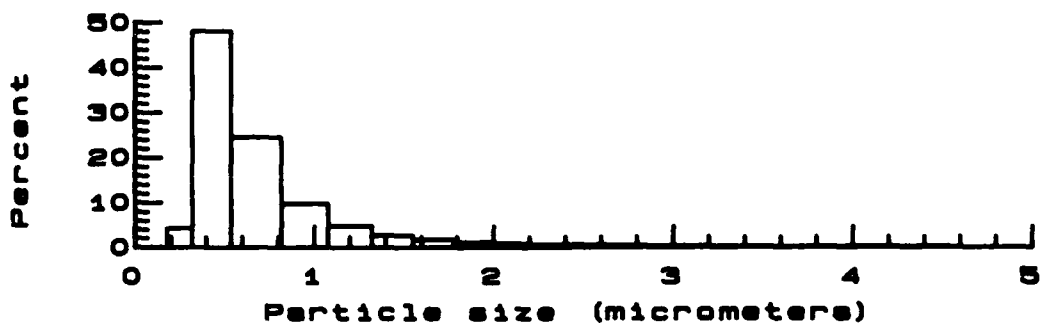


(a) Gas velocity distribution.

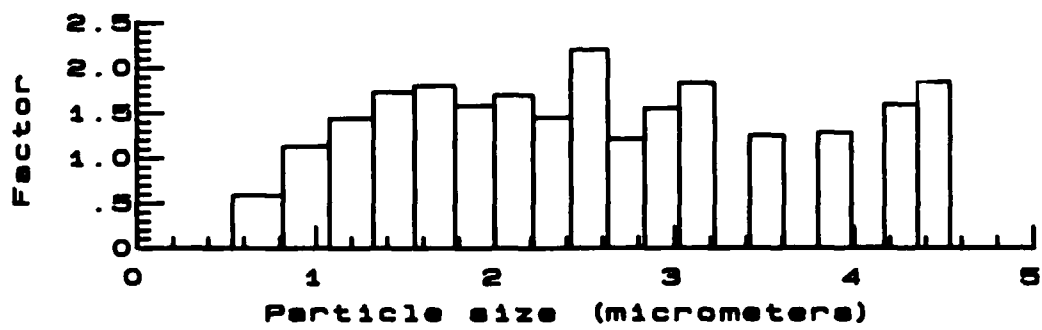


(b) Measured velocity distribution.

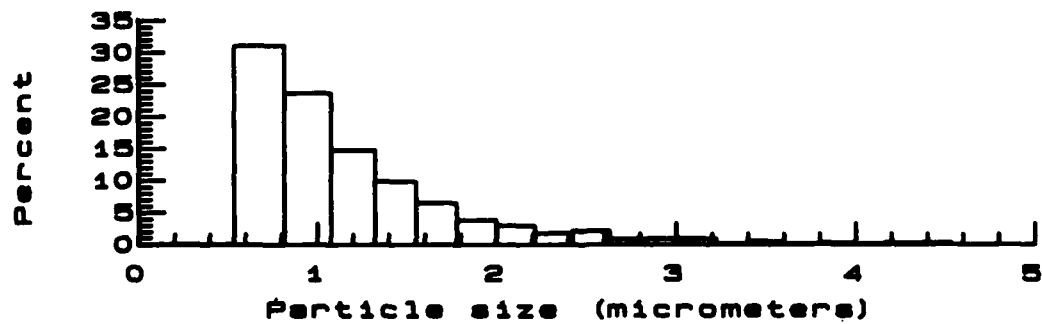
Figure 16.- Illustration of effect of a uniform polydisperse particle size distribution on measured velocity distribution. (Vertical hatching is the spread of velocity due to turbulence.)



(a) Particle size distribution.

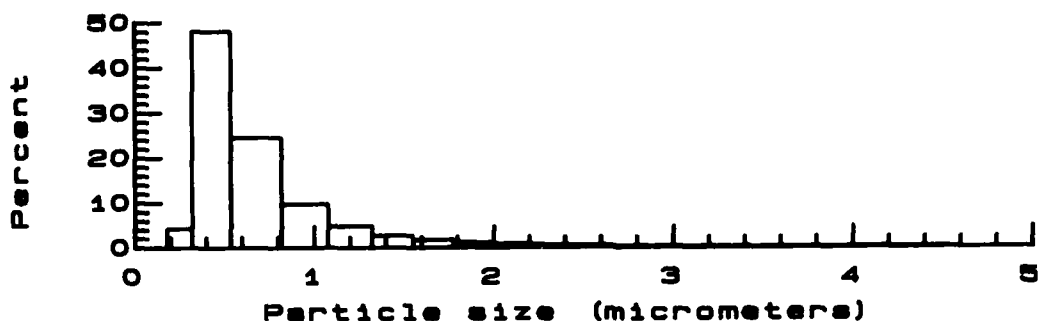


(b) LV sensitivity factors.

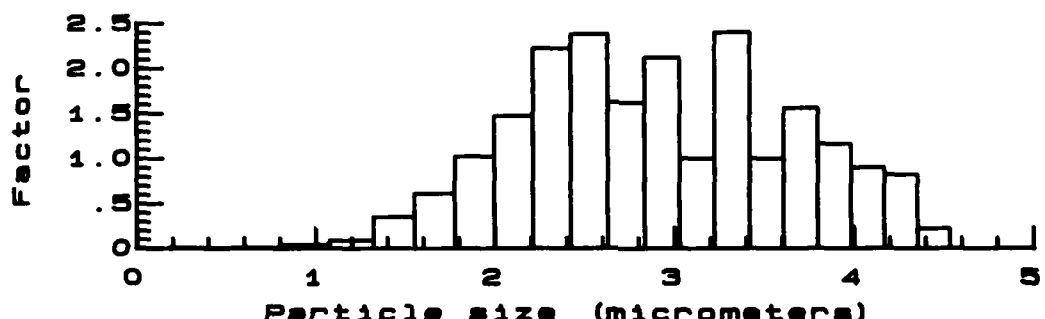


(c) Detectable particle size distribution.

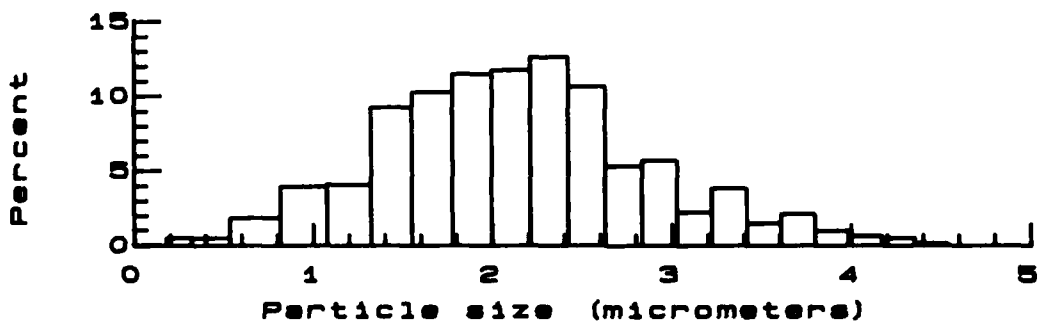
Figure 17.- Kaolin particle size distribution determined by aerodynamic particle size analyzer (converted to histogram widths of the optical particle size analyzer), theoretical LV measurement sensitivity, and detectable particle size distribution.



(a) Particle size distribution.



(b) Estimated LV sensitivity factors.



(c) Estimated detectable particle distribution.

Figure 18.- Kaolin particle size distribution determined from aerodynamic particle size analyzer (see fig. 17(a)), estimated LV measurement sensitivity, and detectable particle size distribution determined by a deconvolution of the measured velocity histogram at $x/D = -0.4$ and -0.5 and the predicted particle velocities.

1. Report No. NASA TP-2502 AVSCOM TR 85-B-4	2. Government Accession No. <i>AD-A163 240</i>	3. Recipient's Catalog No.	
4. Title and Subtitle Performance Test of Laser Velocimeter System for the Langley 16-Foot Transonic Tunnel		5. Report Date December 1985	
7. Author(s) James F. Meyers, William W. Hunter, Jr., David E. Reubush, Cecil E. Nichols, Jr., Timothy E. Hepner, and Joseph W. Lee		6. Performing Organization Code 505-31-53-13	
9. Performing Organization Name and Address NASA Langley Research Center and Aerostructures Directorate USAARTA-AVSCOM Hampton, VA 23665-5225		8. Performing Organization Report No. L-15940	
12. Sponsoring Agency Name and Address National Aeronautics and Space Administration Washington, DC 20546-0001 and U.S. Army Aviation Systems Command St. Louis, MO 63120-1798		10. Work Unit No.	
15. Supplementary Notes James F. Meyers, William W. Hunter, Jr., David E. Reubush, Cecil E. Nichols, Jr., and Joseph W. Lee: Langley Research Center, Hampton, Virginia. Timothy E. Hepner: Aerostructures Directorate, USAARTA-AVSCOM.		11. Contract or Grant No.	
16. Abstract An investigation in the Langley 16-Foot Transonic Tunnel has been conducted in which a laser velocimeter was used to measure free-stream velocities from Mach 0.1 to 1.0 and the flow velocities along the stagnating streamline of a hemisphere-cylinder model at Mach 0.8 and 1.0. The flow velocity was also measured at Mach 1.0 along the line 0.533 model diameters below the model. These tests determined the performance characteristics of the dedicated two-component laser velocimeter at flow velocities up to Mach 1.0 and the effects of the wind tunnel environment on the particle-generating system and on the resulting size of the generated particles. To determine these characteristics, the measured particle velocities along the stagnating streamline at the two Mach numbers were compared with the theoretically predicted gas and particle velocities calculated using a transonic potential flow method. Through this comparison the mean detectable particle size ($2.1 \mu\text{m}$) along with the standard deviation of the detectable particles ($0.76 \mu\text{m}$) was determined; thus the performance characteristics of the laser velocimeter were established. <i>Very good</i>		13. Type of Report and Period Covered Technical Paper	
17. Key Words (Suggested by Author(s)) Laser Laser velocimetry Transonic flows Particle sizing		18. Distribution Statement Unclassified - Unlimited	
<i>Very good</i>			
19. Security Classif. (of this report) Unclassified	20. Security Classif. (of this page) Unclassified	21. No. of Pages 36	22. Price A03

END

FILMED

2-86

DTIC